

3D-Ising-type Magnetic Interactions Stabilized by the Extremely Large Uniaxial Magnetocrystalline Anisotropy in Layered Ferromagnetic Cr_2Te_3

Shubham Purwar, Tushar Kanti Bhowmik, Soumya Ghorai and Setti Thirupathaiah

Department of Condensed Matter and Materials Physics S. N. Bose National Centre for Basic Sciences Kolkata West Bengal 700106 India.

ARTICLE INFO

Keywords:

Layered materials
3D Ising-type magnetic interactions
Magnetocrystalline anisotropy
Critical analysis
Magnetic entropy change

ABSTRACT

We investigate the magnetocrystalline anisotropy, critical behavior, and magnetocaloric effect in ferromagnetic-layered Cr_2Te_3 . We have studied the critical behavior around the Curie temperature (T_C) using various techniques, including the modified Arrott plot (MAP), the Kouvel-Fisher method (KF), and critical isothermal analysis (CI). The derived critical exponents $\beta = 0.353(4)$ and $\gamma = 1.213(5)$ fall in between the three-dimensional (3D) Ising and 3D Heisenberg type models, suggesting complex magnetic interactions by not falling into any single universality class. On the other hand, the renormalization group theory, employing the experimentally obtained critical exponents, suggests 3D-Ising-type magnetic interactions decaying with distance as $J(r) = r^{-4.89}$. We also observe an extremely large uniaxial magnetocrystalline anisotropy energy (MAE) of $K_u = 2065 \text{ kJ/m}^3$, the highest ever found in any Cr_xTe_y based systems, originating from the noncollinear ferromagnetic ground state as predicted from the first-principles calculations. The self-consistent renormalization theory (SCR) suggests Cr_2Te_3 to be an out-of-plane itinerant ferromagnet. Further, a maximum entropy change of $-\Delta S_M^{\text{max}} \approx 2.08 \text{ J/kg-K}$ is estimated around T_C for the fields applied parallel to the c -axis.

1. Introduction

The discovery of intrinsic long-range ferromagnetism in two-dimensional (2D) layered materials has ignited considerable research interest due to their potential technological applications in low-power spintronic devices [1–6]. On the other hand, the Mermin-Wagner theorem proposes certain limitations to have long-range ferromagnetic interactions in the 2D magnets due to thermal fluctuations at finite temperatures [7]. In this regard, the magnetocrystalline anisotropy energy (MAE) becomes crucial to overcome the thermal fluctuations and for the realization of 2D long-range ferromagnetism in layered materials. Recent investigations have focused on enhancing the long-range magnetic ordering in several 2D layered magnets such as CrI_3 [8], $\text{Cr}_2\text{Ge}_2\text{Te}_6$ [9], and $\text{Cr}_2\text{Si}_2\text{Te}_6$ [10]. Nevertheless, the peculiar magnetic behavior observed in chromium-based tellurides (Cr_xTe_y) have drawn significant research attention [11–13].

Under different synthesis conditions and chromium concentrations, Cr_xTe_y exhibits diverse crystal structures owing to the Cr vacancies. For instance, CrTe , Cr_5Te_6 , and Cr_7Te_8 exhibit hexagonal crystal structure [14–16], Cr_3Te_4 and Cr_5Te_8 show monoclinic phase [17–19], and Cr_2Te_3 and CrTe_2 show trigonal crystal structure [20, 21]. Thus, the crystal structure of Cr_xTe_y is highly sensitive to the Cr concentration present in the system, *viz.* Cr_5Te_8 shows monoclinic phase for 38.5 - 40.4 % of Cr, while it shows trigonal structure for 38 - 37.5 % of Cr [22]. Moreover, the Cr concentration significantly affects the magnetic properties as well. Though most of the Cr_xTe_y systems show

ferromagnetic (FM) ordering, CrTe_3 ($\text{Cr}_{0.67}\text{Te}_2$) exhibits an antiferromagnetic ordering [23], their Curie temperatures are highly sensitive to the Cr concentration. For instance, Cr_5Te_8 ($\text{Cr}_{1.25}\text{Te}_2$) shows FM order below $T_C \approx 230 \text{ K}$ [13, 24], Cr_3Te_4 ($\text{Cr}_{1.5}\text{Te}_2$) shows FM order below $T_C \approx 316 \text{ K}$ [17], Cr_7Te_8 ($\text{Cr}_{1.75}\text{Te}_2$) shows FM order below $T_C \approx 361 \text{ K}$ [14], CrTe_2 shows FM order below $T_C \approx 310 \text{ K}$ [20], and Cr_2Te_3 ($\text{Cr}_{1.33}\text{Te}_2$) shows FM order below $T_C \approx 180 \text{ K}$ [21]. Not only the Curie temperature, the magnetic exchange interactions below the Curie temperature are also sensitive to the Cr concentrations. For instance, below T_C , Cr_5Te_8 shows 3D-Ising type magnetic interactions, Cr_4Te_5 shows 3D-Heisenberg type magnetic interactions [11], and CrTe shows quasi-2D-Heisenberg type magnetic interactions [16].

Although the ground state magnetism of Cr_2Te_3 single crystals has been discussed earlier [25], no study is available on Cr_2Te_3 discussing the magnetic exchange interactions across the Curie temperature. Furthermore, Cr_2Te_3 thin films have exhibited an anomalous Hall effect [26, 27], while the topological Hall effect has been observed in heterojunction devices [28]. Thus, a better understanding of the magnetic interactions in Cr_2Te_3 is crucial to unravel the potential technological applications of these systems.

In this contribution, we discuss the magnetocrystalline anisotropy, critical behavior, and magnetocaloric effect in Cr_2Te_3 . The critical behavior around the Curie temperature (T_C) has been studied using various techniques such as the modified Arrott plot (MAP), the Kouvel-Fisher method (KF), and critical isothermal analysis (CI). Interestingly, the derived critical exponents $\beta = 0.353(4)$ and $\gamma = 1.213(5)$ suggest complex magnetic interactions falling in between the 3D Ising and 3D Heisenberg models across the T_C . On the other hand, the renormalization group theory suggests

✉ setti@bose.res.in (S. Thirupathaiah)
www.qmat.in (S. Thirupathaiah)
ORCID(s): 0000-0003-1258-0981 (S. Thirupathaiah)

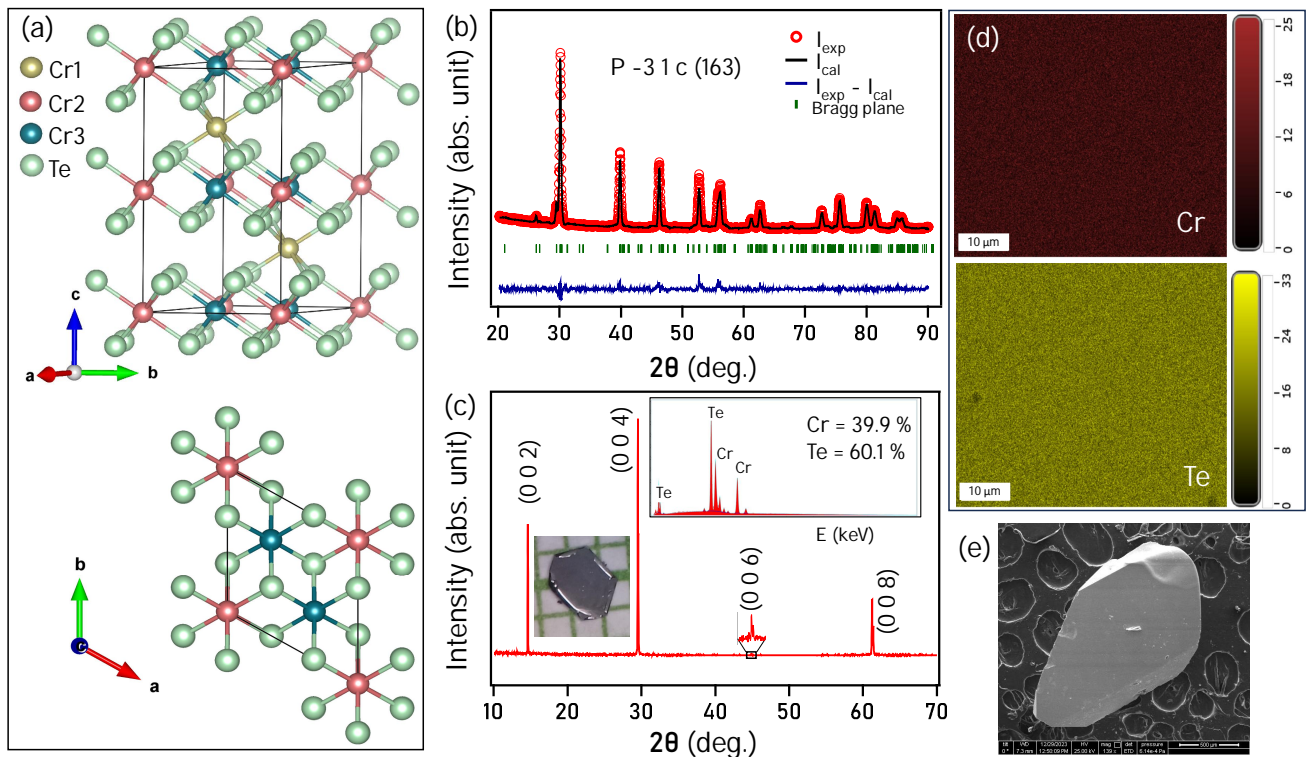


Figure 1: (a) Schematic representations of the Cr_2Te_3 crystal structure, obtained from the Rietveld refinement. (b) XRD pattern of Cr_2Te_3 crushed crystals measured at 300 K overlapped with the Rietveld refinement. (c) XRD pattern of Cr_2Te_3 single crystal. Insets in (c) show EDXS data demonstrating the actual chemical composition of as-prepared crystals and the photographic image of a typical Cr_2Te_3 single crystal. (d) Elemental mapping of Cr_2Te_3 for Cr and Te using EDXS. (e) Scanning electron microscopic (SEM) image of Cr_2Te_3 single crystal.

3D-Ising type magnetic interactions stabilized by the extremely large magnetocrystalline anisotropy. We performed first-principles calculations to establish the origin of extremely large out-of-plane magnetic anisotropy. Our calculations predict a noncollinear ferromagnetic phase with a canted spin structure that results from the magnetic frustration [29], in the ground state with dominant ferromagnetic ordering along the c -axis, while an antiferromagnetic ordering is found in the ab -plane, leading to extremely large magnetocrystalline anisotropy. Further, a maximum entropy change of $-\Delta S_M^{\max} \approx 2.08 \text{ J/kg} - \text{K}$ is estimated around T_C for the fields applied parallel to the c -axis.

2. Experimental and First-principles Calculation Details

High-quality single crystals of Cr_2Te_3 were grown using the chemical vapor transport (CVT) technique by taking 3 : 4 molar ratio of Chromium (Cr, 99.99%, Alfa Aesar) and Tellurium (Te, 99.999%, Alfa Aesar) powders and employing iodine as the transport agent. The growth process involved a three-week thermal heat treatment in a two-zone horizontal tube furnace, with the source-zone maintained at 1000 °C and the growth-zone kept at 820 °C [30]. The as-grown single crystals, sized $3 \times 2 \text{ mm}^2$, were looking shiny and flat [see the inset of Fig. 1(c)]. Surface morphology and

elemental compositions were studied by using the scanning electron microscope (SEM) and energy dispersive x-ray spectroscopy (EDXS). We find that the as-prepared single crystals have a Cr to Te ratio of 0.663(6):1, leading to the exact chemical formula of $\text{Cr}_{1.99}\text{Te}_3$. Powder x-ray diffraction (XRD) analysis was conducted using a Rigaku X-ray diffractometer (SmartLab, 9kW) with Cu K_α radiation (wavelength = 1.5406 Å). Magnetic properties studies, $M(T)$ and $M(H)$, were performed using the physical property measurement system (PPMS, 9 Tesla DynaCool, Quantum Design). The magnetization isotherms $M(H)$ were systematically measured with 2 K interval around the Curie temperature to facilitate the critical behavior analysis.

Density functional theory (DFT) calculations on Cr_2Te_3 were performed using the generalized gradient approximation (GGA) of Perdew, Burke and Ernzerhof (PBE) exchange and correlation functionals [31] as implemented in the Quantum Espresso (QE) simulation package [32]. Brillouin zone sampling was done over a $12 \times 12 \times 6$ Monkhorst-Pack k -grid. The electronic wave function is expanded using the plane waves up to a cutoff energy of 40 Ry. To accurately determine the spin moment distribution, our approach involved incorporating scalar-relativistic and relativistic pseudopotentials to account the within the self-consistent field (SCF) calculations. We explored both collinear and non-collinear spin

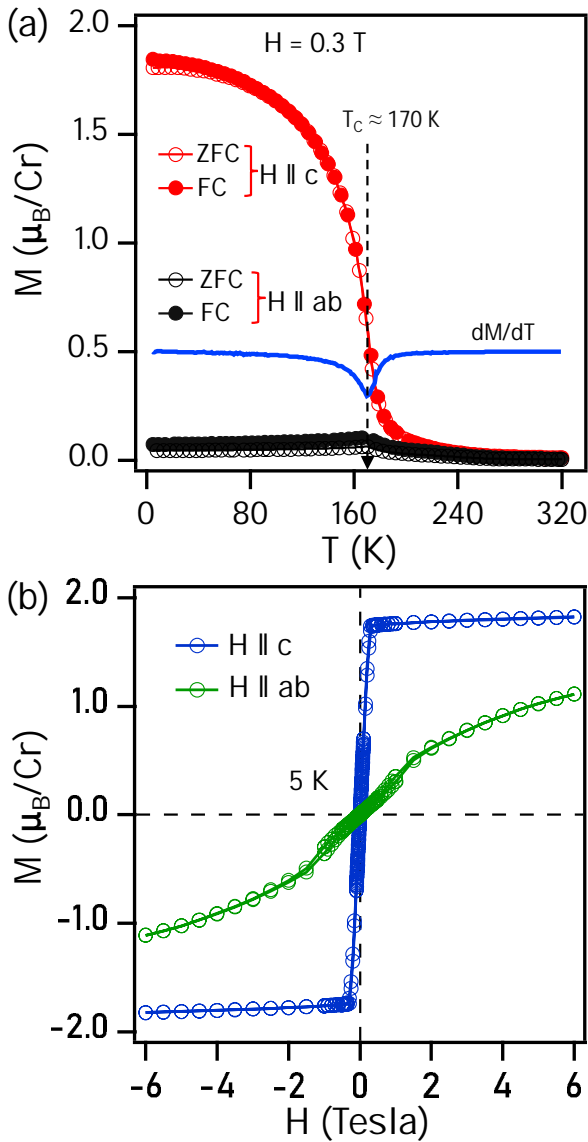


Figure 2: (a) Temperature-dependent magnetization $M(T)$ measured for $H \parallel c$ and $H \parallel ab$ in the ZFC and FC modes under an applied of $H = 0.3$ T. In (a), the blue-curve displays first derivative of magnetization with respect to temperature, $\frac{dM}{dT}$, showing a dip at the $T_C \approx 170$ K. (b) Magnetization isotherms [$M(H)$] measured at 5 K for $H \parallel c$ and $H \parallel ab$ orientations.

structures, the latter involving optimization of the spin angle with respect to the energy.

3. Results and Discussion

3.1. Structural analysis

The unit cell of Cr_2Te_3 is schematically shown in the top-panel of Fig. 1(a), in which distinct chromium atoms are labeled by Cr(1), Cr(2), and Cr(3). The intercalated Cr(1) atoms reside within the van der Waals gap created by two CrTe_2 layers, exhibiting ordered vacancies. Cr(2) and Cr(3) are within the CrTe_2 layers, but only Cr(3) has the nearest neighboring Cr(1) atoms along the c -axis. On the other hand,

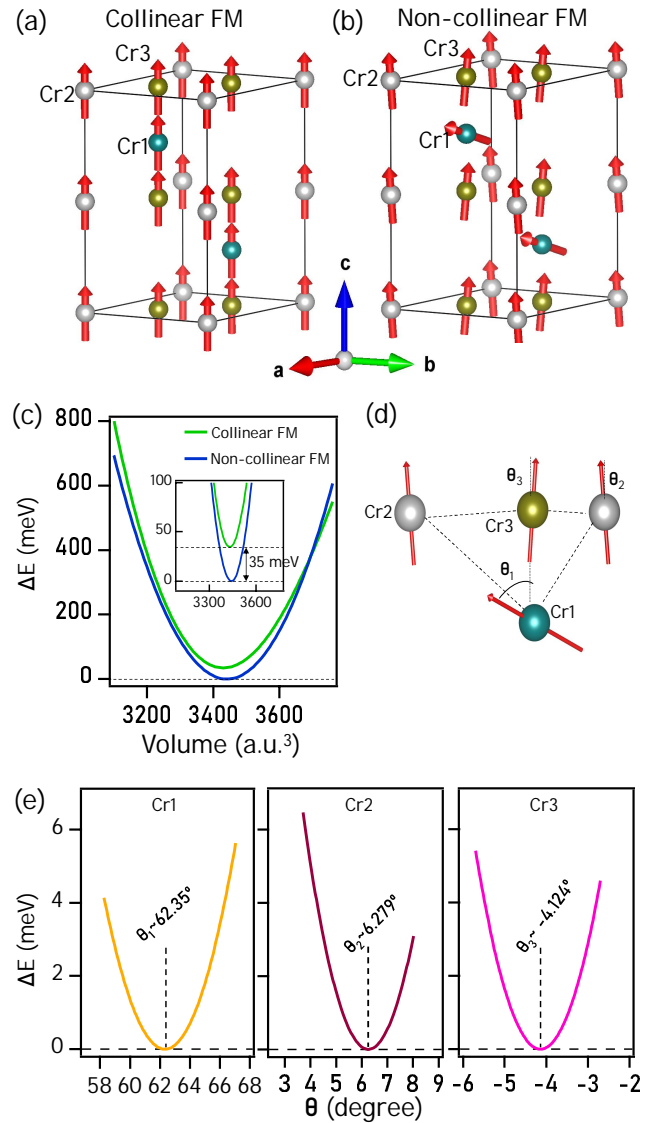


Figure 3: Schematic representations of the collinear ferromagnetic (FM) (a) and noncollinear ferromagnetic (b) configurations. (c) Relative total energy (ΔE), with respect to the ground state energy, plotted as a function of unit cell volume for both magnetic configurations, obtained using the DFT calculations. (d) Schematic diagram of the canting spin angles of Cr(1), Cr(2), and Cr(3) atoms with respect to the c -axis. (e) Relative total energy (ΔE), with respect to the ground state energy, plotted as a function of spin angles for Cr(1), Cr(2) and Cr(3) atoms.

Cr(1) has two Cr(3) nearest neighbours along the c -axis but has no nearest neighbors in the ab -plane. The bottom-panel of Fig. 1(a) depicts projected crystal structure of Cr_2Te_3 onto the ab -plane, showing the intertwined honeycomb lattice with Cr(2), Cr(3), and Te atoms. Fig. 1(b) displays the X-ray diffraction (XRD) pattern of the crushed single crystals measured at room temperature. The XRD data confirms the trigonal crystal structure of Cr_2Te_3 having the space group of $P\bar{3}1c$ (163). The derived lattice parameters using the Rietveld refinement, $a = b = 6.7989(7)$ Å, $c = 12.1074(7)$

Å, and the angles $\alpha = \beta = 90^\circ$, $\gamma = 120^\circ$, are close to the previous reports [18, 22, 33]. Fig. 1(c) displays the XRD pattern taken on the Cr_2Te_3 single crystal, indicating that the crystal growth is parallel to the (00 l) Bragg's plane. Using the Rietveld refinement, bond lengths of $\text{Cr}_1\text{-Cr}_3$, $\text{Cr}_2\text{-Cr}_3$, $\text{Cr}_2\text{-Cr}_2$, and $\text{Cr}_3\text{-Cr}_3$ are determined as 3.0269 Å, 3.9254 Å, 6.7990 Å, and 3.9254 Å, respectively. Additionally, the bond angles of $\text{Cr}_2\text{-Te}_1\text{-Cr}_3$, $\text{Cr}_1\text{-Te}_1\text{-Cr}_2$, and $\text{Cr}_1\text{-Te}_1\text{-Cr}_3$ are found as 91.213° , 129.596° , and 67.542° , respectively. Fig. 1(d) exhibits the elemental mapping of Cr and Te, confirming the uniform chemical composition of the studied crystal within the measured surface range of $50 \times 45 \text{ } (\mu\text{m})^2$. Fig. 1(e) shows scanning electron microscopy (SEM) image of Cr_2Te_3 , displaying a very flat surface morphology. Thus, the EDXS and SEM data confirm the homogeneity and high-quality of the studied single crystals.

3.2. Magnetic Properties

Temperature-dependent magnetization [$M(T)$] of Cr_2Te_3 measured at $H = 0.3 \text{ T}$ for both the $H \parallel c$ and $H \parallel ab$ orientations are shown in Fig. 2(a) taken in field-cooled (FC) and zero-field-cooled (ZFC) modes. From Fig. 2(a), we observe a ferromagnetic-like magnetic transition at around $T_C \approx 170 \text{ K}$. The same is confirmed from the overlapped dM/dT data in which a dip is noticed at around 170 K. Most interestingly, we observe an out-of-plane ($H \parallel c$) saturation magnetization ($1.8 \mu_B/\text{Cr}$) that is almost 20 times higher than the in-plane ($H \parallel ab$) saturation magnetization ($0.08 \mu_B/\text{Cr}$), indicating an extremely large magnetic anisotropy in this system with an easy-axis of magnetization parallel to the c -axis. To further confirm the magnetic anisotropy, we measured magnetization as a function of the field [$M(H)$] for both orientations as shown in Fig. 2(b) at 5 K of the sample temperature. From Fig. 2(b), we clearly notice a spontaneous magnetization of $1.8 \mu_B/\text{Cr}$ for $H \parallel c$ around the zero applied field with negligible coercivity, suggesting Cr_2Te_3 to be an out-of-plane soft-ferromagnet. On the other hand, for $H \parallel ab$, the lower magnetic fields sustain a canted FM state between neighboring Cr(2) and Cr(3) atoms.

We performed density functional theory (DFT) calculations to reveal the ground state magnetic structure of Cr_2Te_3 . Initially we focused on examining the magnetic coupling among various types of Cr atoms, including the collinear ferromagnetic (FM) and non-collinear FM configurations as shown in Figs. 3(a) and 3(b), respectively. The DFT calculations are done by including the spin-orbit coupling (SOC) effect. Our calculations suggest that the noncollinear ferromagnetic configuration [see Fig. 3(c)] has a lower ground state energy by about 35 meV compared to the collinear FM configuration, thus the former is a more stable magnetic ground state than the latter in Cr_2Te_3 . Distinct spin canting angles were observed for Cr(1), Cr(2), and Cr(3) deviating from the c -axis as schematically shown in Fig. 3(d). This investigation suggests substantial difference in the canted spin angles, between the intercalated Cr(1) atoms and Cr(2) or Cr(3) of CrTe_2 layer [21]. Further, Cr(1) and Cr(2) display spin canting in the second quadrant, while Cr(3) exhibits

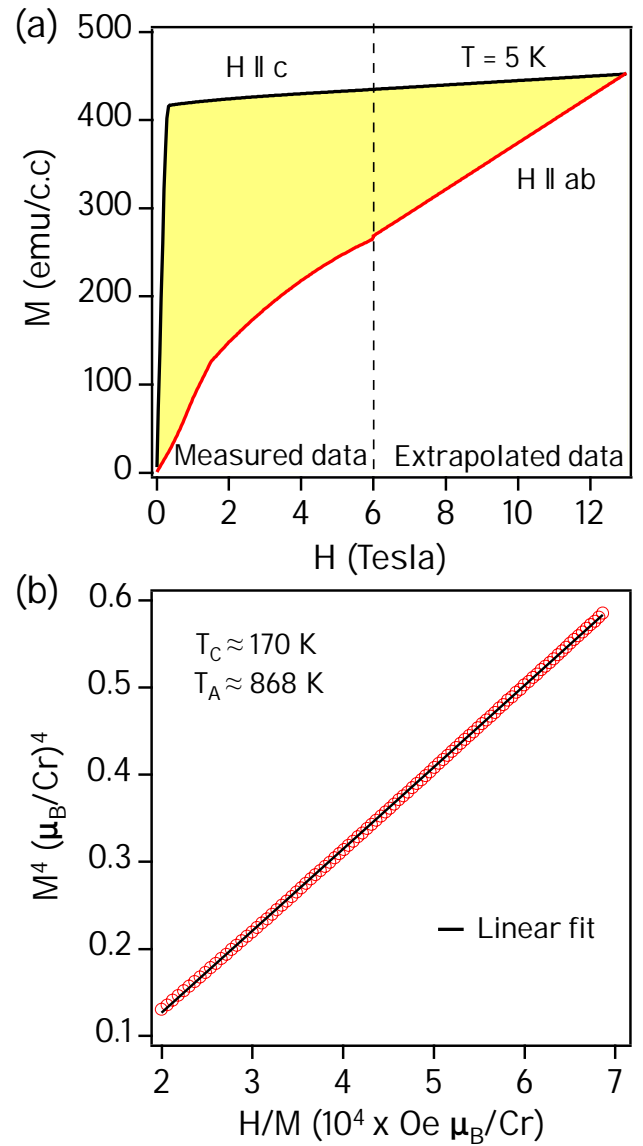


Figure 4: (a) Magnetization isotherms [$M(H)$] measured at 5 K for $H \parallel c$ and $H \parallel ab$. The yellow shaded area represents the magnetocrystalline anisotropy energy (MAE). (b) Plot of M^4 vs. H/M

spin canting in the first quadrant, as depicted in Fig. 3(d). Fig. 3(e) depicts the plots of relative total energy (ΔE) vs. spin canting angle, suggesting 62.35° , 6.279° , and -4.124° are the canted-spin angles of Cr(1), Cr(2), and Cr(3) atoms, respectively in the magnetic ground state. Therefore, the predicted canted angles indicate a dominant ferromagnetic ordering for the spins of Cr(2) & Cr(3) of CrTe_2 layer and a dominant antiferromagnetic ordering for the intercalated Cr(1) atoms. As a result, the noncollinear FM ground state in Cr_2Te_3 is stabilized by the magnetic frustration due to a competition between the in-plane AFM and the out-of-plane FM orders. These observations are consistent with predictions on similar systems [21, 34].

Next, with the help of magnetization isotherms [$M(H)$] measured at 5 K for both $H \parallel c$ and $H \parallel ab$ [see

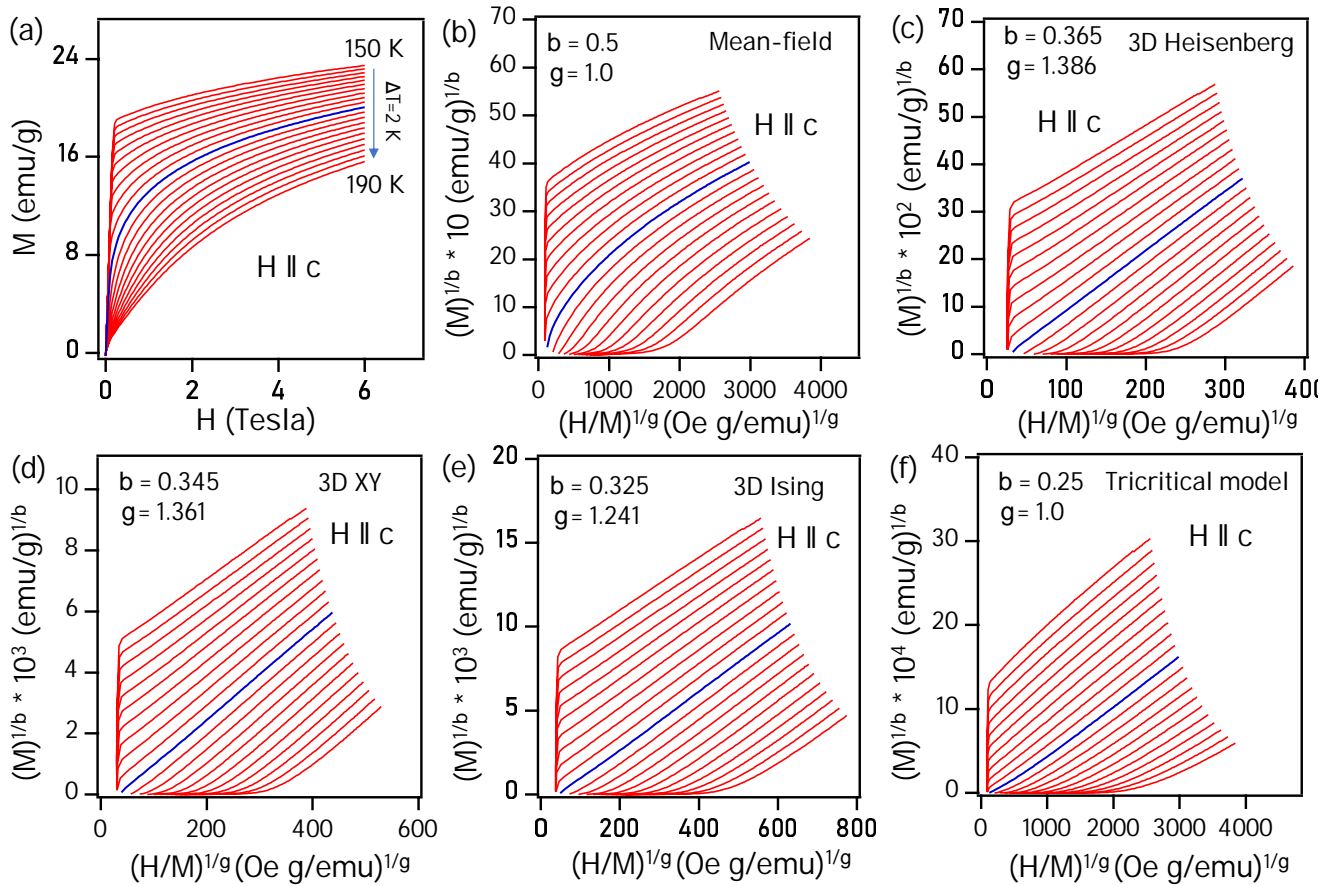


Figure 5: (a) Isothermal magnetization $M(H)$ measured between 150 and 190 K with an interval of 2 K for $H \parallel c$. (b) Arrott plots of M^2 vs. (H/M) for the Landau mean-field model. Modified Arrott plots of $M^{1/b}$ vs. $(H/M)^{1/g}$ for (c) 3D-Heisenberg model, (d) 3D-XY model, (e) 3D-Ising model, and (f) Tricritical mean-field model. In the figures, the blue-colored data is taken at the $T_C \approx 170$ K.

Fig. 4(a)], we qualitatively estimated the magnetocrystalline anisotropy energy (MAE) K_u in our studied Cr_2Te_3 sample by measuring the area (Yellow-shaded region) between $H \parallel c$ and $H \parallel ab$ curves, using the relation [19],

$$K_u = \mu_0 \int_0^{M_s} [H_c(M) - H_{ab}(M)] dM \quad (1)$$

Here, μ_0 is the vacuum permeability, M_s represents saturation magnetization. H_c and H_{ab} represent magnetic field applied along the out-of-plane and in-plane directions, respectively.

The derived value of $K_u = 2065 \text{ kJ/m}^3$ in this method is found to be the highest ever known MAE from any Cr_xTe_y type systems. Moreover, this value is much larger than the K_u values reported on many other 2D magnetic systems such as $\text{Cr}_2\text{Si}_2\text{Te}_6 / \text{Cr}_2\text{Ge}_2\text{Te}_6$ ($\approx 65 \text{ kJ/m}^3 / \approx 20 \text{ kJ/m}^3$) [35], Fe_4GeTe_2 (250 kJ/m^3) [36], $\text{CrBr}_3 / \text{CrI}_3$ ($\approx 86 \text{ kJ/m}^3 / \approx 300 \text{ kJ/m}^3$) [37], and Fe_3GeTe_2 (1460 kJ/m^3) [38]. Thus, for the first-time we report an extremely large MAE from our studied Cr_2Te_3 . Note here that we estimated the MAE value by linearly extrapolating the high-field region of the $M(H)$ data for $H \parallel ab$ [see Fig. 4(a)] to find the

overlapping field position (12.8 T) with $H \parallel c$. Therefore, the MAE value $K_u = 2065 \text{ kJ/m}^3$ is the minimum value that we could estimate in this method. The actual K_u value would be higher than what we estimated, if one is able to perform $M(H)$ measurements at very high applied magnetic fields and find the overlapping field position directly from the measurements. Nevertheless, we could also estimate the magnetocrystalline anisotropy energy using the DFT calculations. In agreement with the experimental value, we find an extremely large MAE for the noncollinear FM state of 8230 kJ/m^3 . Whereas for the collinear FM state we find relatively very low MAE of 32 kJ/m^3 .

3.3. Itinerant Ferromagnetism

To identify the nature of ferromagnetism in Cr_2Te_3 we employed Takahashi's self-consistent renormalization (SCR) theory which takes into account the conservation of zero-point spin fluctuations and thermal spin fluctuations [39]. According to SCR theory, the magnetization M and the magnetic field H at T_C should obey the below

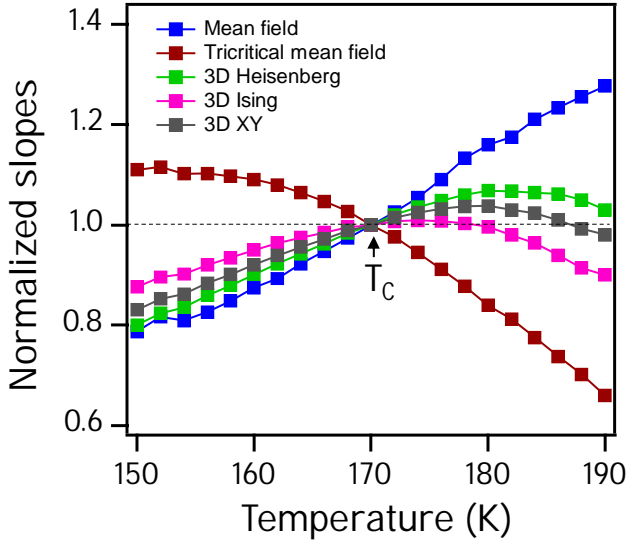


Figure 6: Temperature dependent normalized slopes [$NS=S(T)/S(T_C)$] plotted as a function of temperature, for various models, derived from the data shown in Figs. 5(b) - 5(f). See the text for more details.

relation,

$$M^4 = \frac{1}{4.671} \left[\frac{T_C^2}{T_A^3} \right] \left(\frac{H}{M} \right) \quad (2)$$

Here, T_A is the dispersion of the spin fluctuation spectrum in wave-vector space. T_A , M , and H are in K, μ_B/Cr , and Oe units, respectively. Fig. 4(b) shows the plot of M^4 vs. H/M , fitted by Eq. 2. Such a linear behavior is observed in many itinerant ferromagnets such as MnSi [40], LaCo_2P_2 [41], SmCoAsO [42]. From the fitting of Eq. 2, we obtained a slope of $9.4778 \times 10^{-6} (\mu_B/\text{Cr})^5/\text{Oe}$. Using the slope and $T_C \approx 170$ K, we derived $T_A \approx 868$ K for $H \parallel c$.

Further, following the SCR theory, T_C can be expressed by,

$$T_C = (60c)^{-3/4} P_S^{3/2} T_A^{3/4} T_0^{1/4} \quad (3)$$

Here, $c = 0.3353$, P_S is the spontaneous magnetization in μ_B/Cr , T_0 is the energy width of the dynamical spin fluctuation spectrum in K. Using the value of T_C , P_S , and T_A , we obtain the characteristic temperature $T_0 = 4502$ K for our Cr_2Te_3 single crystal. According to the SCR theory of spin fluctuation, the ratio T_C/T_0 is an important parameter as it characterizes the degree of localization or itineracy of the spin moment. The magnetic materials are found to exhibit itinerant character for $T_C/T_0 \ll 1$, while they show localized magnetism for $T_C/T_0 \approx 1$. In our case of Cr_2Te_3 single crystal, the ratio T_C/T_0 is estimated to be 0.04 which is much smaller than 1, indicating the itinerant nature of the ferromagnetism in Cr_2Te_3 .

3.4. Critical Behaviour Analysis

Investigating the magnetic interactions across the paramagnetic to ferromagnetic transition involves the critical exponents analysis of magnetization isotherms [$M(H)$] around T_C . The $M(H)$ data measured for $H \parallel c$ between 150 and 190 K with an interval of 2 K are depicted in Fig. 5(a). Fig. 5(b) shows Arrott plots of M^2 vs. (H/M) for the Landau mean-field model. Arrott plots typically display a positive slope of parallel lines in the high-field region, indicative of a second-order magnetic transition [43]. However, our findings show deviation from the linear behavior, particularly below T_C . This deviation suggests that the Landau mean-field theory ($\beta = 0.5, \gamma = 1$) is not applicable to Cr_2Te_3 . Consequently, a modified Arrott plot (MAP) is necessary to determine the critical exponents by following the below equation,

$$(H/M)^{1/\gamma} = a * (T - T_C)/T_C + b * M^{1/\beta} \quad (4)$$

where (H/M) is the inverse susceptibility, M is the magnetization, T_C is Curie temperature, β and γ are the critical exponents, and a and b are constants.

Scaling hypothesis of the critical phenomena theory [44] suggests that the second-order phase transitions near T_C are governed by the critical exponents and magnetic equations of the state. The divergence of the correlation length around T_C , $\xi = \xi_0[(T - T_C)/T_C]^{-\nu}$, gives rise to universal scaling laws. This results in specific critical exponents β for spontaneous magnetization M_{sp} below T_C , γ for the inverse susceptibility χ_0^{-1} above T_C , and δ for magnetization isotherms $M(H)$ at T_C which are mathematically represented in the magnetic equations involving these critical exponents,

$$M_{sp}(T) = M_0(-\epsilon)^\beta \text{ for } \epsilon < 0, T < T_C, \quad (5)$$

$$\chi_0^{-1}(T) = (h_0/m_0)\epsilon^\gamma, \text{ for } \epsilon > 0, T > T_C \quad (6)$$

$$M = DH^{1/\delta}, \text{ for } \epsilon = 0, T = T_C, \quad (7)$$

where $\epsilon = (T - T_C)/T_C$ is the reduced temperature, M_0 , h_0/m_0 , and D are the critical amplitudes [49]. Attempts were made to derive the critical exponents and T_C through MAP technique by plotting $M^{1/\beta}$ vs. $(H/M)^{1/\gamma}$ based on various theoretical models around T_C such as the 3D-Heisenberg model, 3D-XY model, 3D-Ising model, and tricritical mean-field model [45, 46, 50] as shown in Figs. 5(c), 5(d), 5(e), and 5(f), respectively. However, none of these models produced the anticipated parallel lines. To further confirm that none of these models can adequately describe the magnetic interactions of this system, in Fig. 6 we plotted the normalized slopes (NS), $NS = S(T)/S(T_C)$, as a function of temperature at higher magnetic fields derived from the data shown in Figs. 5(b)- 5(f) for various models. Here, $S(T)$

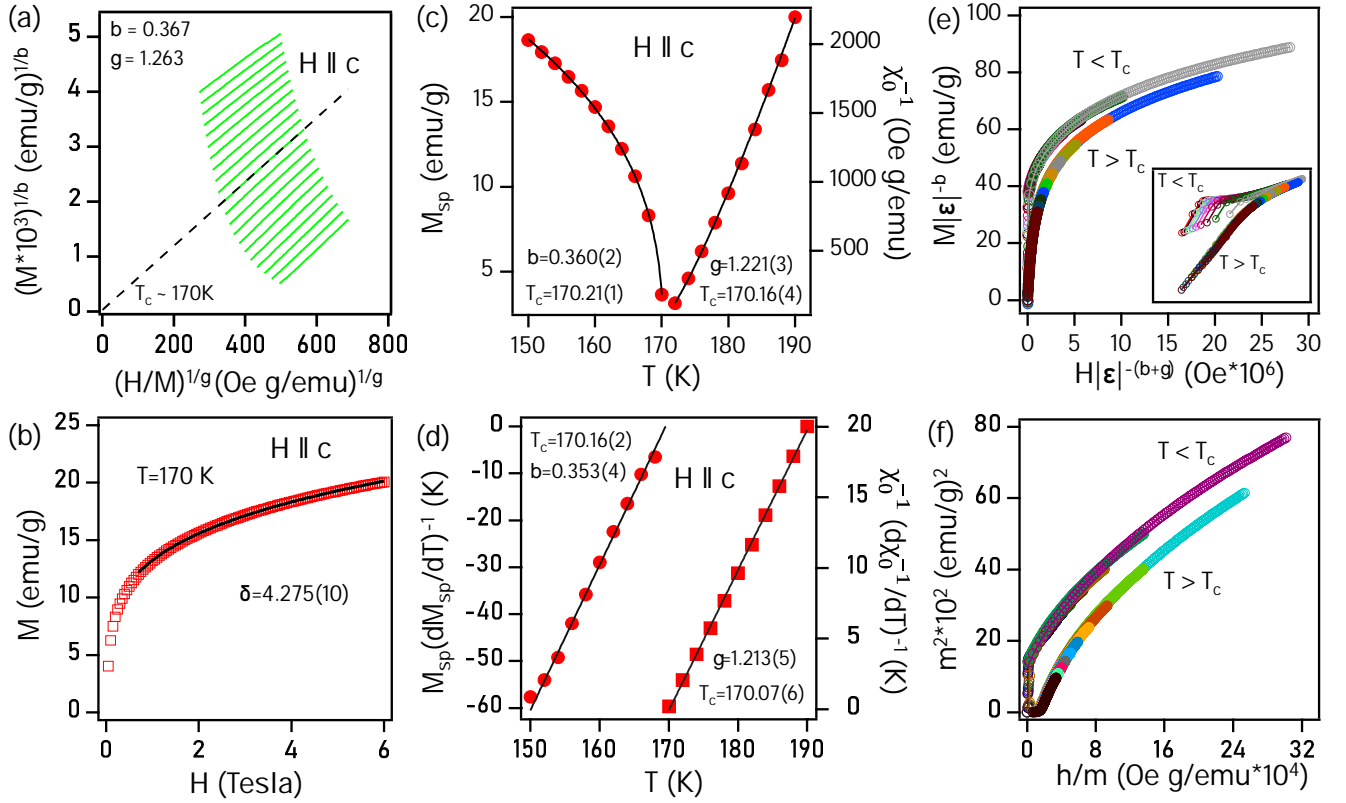


Figure 7: (a) Modified Arrott plot (MAP) of $M^{1/\beta}$ vs. $(H/M)^{1/\gamma}$ at high-field regions with critical exponents, $\beta = 0.367$ and $\gamma = 1.263$. (b) Isothermal magnetization $M(H)$ data taken at $T_C = 170$ K (c) Temperature dependent spontaneous magnetization $M_{sp}(T)$ (left axis) and inverse initial susceptibility $\chi_0^{-1}(T)$ (right axis). (d) Kouvel-Fisher plot: temperature dependence of $M_{sp}(T)[dM_{sp}(T)/dT]^{-1}$ (left axis) and $\chi_0^{-1}(T)[d\chi_0^{-1}(T)/dT]^{-1}$ (right axis). (e) Scaling plot of normalized magnetization vs. normalized field. (f) Renormalized magnetization (m) and field (h) are plotted in the form of m^2 vs. h/m below and above T_C . Inset in (e) shows the same plot of (e) in log-log scale.

is the slope defined by $d(M^{1/\beta})/d((H/M)^{1/\gamma})$ at a given temperature T . For any adequate model, the normalized slopes should be equal to one [47, 48]. However, from Fig. 6 it is evident that none of the models show NS=1 at temperatures other than T_C . Therefore, none of the standard models, Landau mean-field, 3D-Heisenberg, 3D-XY, 3D-Ising, and tricritical mean-field model, can describe the magnetic interactions in Cr_2Te_3 precisely.

Thus, to accurately determine the critical exponents near T_C , an iterative modified Arrott plot (MAP) technique was employed on the data shown in Fig. 5(a) [51, 52]. In this method, we start with trial values of β and γ substituted into Eq. 4 to derive the MAP data as shown in Fig. 7(a). The linear extrapolation of the MAP data from the high field region provides $(M_{sp})^{1/\beta}$ and $(\chi_0^{-1})^{1/\gamma}$ as intercepts on the y and x-axis of the $(M)^{1/\beta}$ vs. $(H/M)^{1/\gamma}$ plot [see Fig. 7(a)]. As obtained M_{sp} and χ_0^{-1} are plotted as a function of temperature as shown in Fig. 7(c). Next, $M_{sp}(T)$ and $\chi_0^{-1}(T)$ are fitted using Eqs. 5 and 6 to determine new β and γ values. Using these updated β and γ exponents, a new MAP is created by plotting $(M)^{1/\beta}$ vs. $(H/M)^{1/\gamma}$. This procedure is iteratively repeated, involving fitting the modified Arrott plots, updating the polynomials (Eqs. 5 and

6), and recalculating the exponents, until the values of β and γ converge ($\beta_{n+1} \rightarrow \beta_n$ and $\gamma_{n+1} \rightarrow \gamma_n$, here n is the iteration number). After this iterative exercise, Fig. 7(a) shows parallel straight lines with $\beta = 0.367$ and $\gamma = 1.263$ in which the straight line corresponding to the T_C passes through the origin. Further, from the converged MAP, the $M_{sp}(T)$ and $\chi_0^{-1}(T)$ are plotted in Fig. 7(c) from which the fittings with Eqs. 5 and 6 derive the critical exponents $\beta = 0.360(2)$ with $T_C = 170.21(1)$ K and $\gamma = 1.221(3)$ with $T_C = 170.16(4)$ K. These T_C values closely match the T_C of 170 K estimated from $M(T)$ data [see Fig. 2(a)].

To verify the accuracy and reliability of the critical exponents determined by the modified Arrott plot method, we employed the Kouvel-Fisher (KF) method [53], using the equations,

$$M_{sp}(T)[dM_{sp}(T)/dT]^{-1} = (T - T_C)/\beta, \quad (8)$$

$$\chi_0^{-1}(T)[d\chi_0^{-1}(T)/dT]^{-1} = (T - T_C)/\gamma, \quad (9)$$

Thus, Fig. 7(d) exhibits KF plots fitted using the Eqs. 8 and 9 both below and above T_C . In this way, we obtained

Table 1

Comparison of critical exponents of Cr_2Te_3 with similar 2D magnetic materials and different theoretical models.

Composition	Technique	T_c	β	γ	δ	Reference
Cr_2Te_3	MAP	170.21(1)	0.360(2)	1.221(3)	4.392(6)	This work
Cr_2Te_3	KF method	170.07(6)	0.353(4)	1.213(5)	4.436(2)	This work
Cr_2Te_3	Critical isotherm	170			4.275	This work
Theory	3D Ising		0.325	1.241	4.82	[45]
Theory	3D XY		0.345	1.316	4.81	[45]
Theory	3D Heisenberg		0.365	1.386	4.80	[45]
Theory	Landau mean-field		0.5	1	3	[43]
Theory	Tricritical mean-field		0.25	1	5	[46]
Cr_5Te_8	KF method	230.6(3)	0.315(7)	1.81(2)	6.35	[47]
Cr_3Te_4	KF method	320.335(5)	0.365(5)	1.212(9)	4.580(4)	[48]
Cr_4Te_5	KF method	319.06(9)	0.387(9)	1.2885(2)	4.32	[11]
Cr_5Te_6	KF method	338.17(1)	0.405(1)	1.200(1)	3.962(9)	[15]

the critical exponents $\beta = 0.353(4)$ with $T_C = 170.16(2)$ K and $\gamma = 1.213(5)$ with $T_C = 170.07(6)$ K, respectively. Notably, these values are very close to the critical exponents obtained from the MAP method, affirming the reliability, self-consistency, and intrinsic nature of the critical exponents. Furthermore, using the Widom scaling relation, $\delta = 1 + (\gamma/\beta)$ [54], we estimate $\delta = 4.392(6)$ and $\delta = 4.436(2)$ from the MAP and KF plots, respectively. Crucially, these δ values, obtained from different methods converge to $\delta = 4.275(10)$ derived through the critical isotherm (CI) method using Eq. 7 [see Fig. 7(b)]. The experimentally derived critical exponents are summarized in Table 1 along with critical exponents of different theoretical models and other Cr_xTe_y systems.

Further, in the critical asymptotic region of magnetic materials, the scaling equation of magnetic state is expressed by [44],

$$M(H, \epsilon) = e^\beta f_\pm(H/\epsilon^{\beta+\gamma}) \quad (10)$$

This equation can also be expressed as,

$$m = f_\pm(h) \quad (11)$$

where $m = \epsilon^{-\beta} M(H, \epsilon)$ denotes the normalized magnetization and $h = H\epsilon^{-(\beta+\gamma)}$ represents the normalized field. When the values of β and γ obtained from both the MAP and KF methods are accurately chosen, the scaled magnetization m and h are expected to mainly fall into to two distinct branches of universal curves outlined by the Eqs. 10 and 11. These branches correspond to temperatures below and above T_C as evident in Figs. 7(e) and 7(f).

The compiled critical exponents in Table 1, compared with theoretical predictions across various models, reveal complex magnetic interactions across the Curie temperature in Cr_2Te_3 . Specifically, the value of β ($T < T_C$) obtained

Table 2

Obtained critical parameters from renormalization group theory

{d : n}	γ	β	σ	δ
{3 : 1}	1.213	0.362	1.888	4.395
{3 : 2}	1.213	0.395	1.827	4.116
{3 : 3}	1.213	0.415	1.791	3.964

from the MAP technique is very close to the 3D-Heisenberg type interactions, while the value of γ ($T > T_C$) is very close to the 3D-Ising type interactions. However, the value of δ obtained at T_C does not fall into any of the existing standard models of 3D-Heisenberg, 3D-XY, or 3D-Ising (See Table 1). The deviation of the magnetic interactions may stem from various factors such as long-range Ruderman-Kittel-Kasuya-Yosida (RKKY) interactions [45], extended interactions beyond nearest neighbors [55], dipole-dipole interaction [56], or strong magnetocrystalline anisotropy (MAE) [57–59]. Thus, it is necessary to understand the range of magnetic interactions and spin dimensionality of Cr_2Te_3 . For a homogeneous magnet, the magnetic phase transition's universality class depends on the exchange interaction $J(r)$ and following the renormalization group (RG) theory the interactions decay with distance as $J(r) = r^{-(d+\sigma)}$. Here, d is the spacial dimensionality and σ is a positive constant. The relation between the critical exponent γ and σ can be expressed by [49, 60],

$$\gamma = 1 + \frac{4(n+2)}{d(n+8)}\Delta\sigma + \frac{8(n-4)(n+2)}{(n+8)^2d^2} * \left[\frac{2(7n+20)G(d/2)}{(n+8)(n-4)} + 1 \right] \Delta\sigma^2 \quad (12)$$

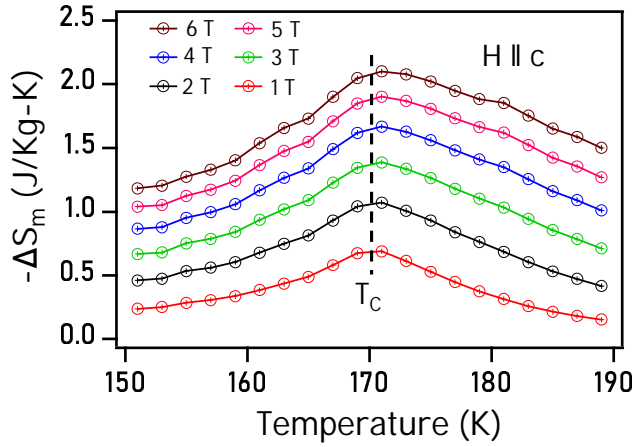


Figure 8: Temperature dependent magnetic entropy change $-\Delta S_m$ at different applied magnetic fields.

where $\Delta\sigma = \sigma - d/2$, $G(d/2) = 3 - 0.25 * (d/2)^2$. n and d are the spin and spatial dimensionality of the system [60]. For $\sigma > 2$, the short-range Heisenberg model is valid for describing a 3D-isotropic magnet with magnetic interactions $J(r)$ decaying faster than r^{-5} . Conversely, for $\sigma \leq 3/2$, the system follows the long-range mean-field model with magnetic interactions $J(r)$ decaying slower than $r^{-4.5}$ [61]. For $3/2 \leq \sigma \leq 2$ the system falls into a distinct category characterized by the critical exponents that vary according to the specific value of σ . According to Eq. 12, it is found that $\{d : n\} = \{3 : 1\}$ and $\gamma = 1.213$ give the critical exponents $\beta = 0.362$, $\sigma = 1.89$, and $\delta = 4.395$ which are close to our experimental observations. The other exponents (ν , α , γ) can be derived from the following scaling equations, $\nu = \gamma/\sigma$, $\alpha = 2 - \nu * d$, $\beta = (2 - \alpha - \gamma)/2$, where ν and α are the exponents of correlation length. This is done for various sets of $\{d : n\}$ values, as shown in Table 2. Thus, the exchange interactions in Cr_2Te_3 decay as $J(r) = r^{-(d+\sigma)} = r^{-4.89}$. The spin dimensionality $n = 1$ and the spacial dimensionality $d = 3$ as derived from the RG theory suggests 3D-Ising type magnetic interactions, stabilized by the robust uniaxial anisotropy present in the system. This behavior mirrors the observations in other Cr_xTe_y systems [47, 62]. Therefore, in Cr_2Te_3 the magnetism primarily arises from the intralayer coupling [63], as evidenced by the 3.9254 \AA bond length between adjacent Cr atoms within the plane, indicative of a relatively weak direct exchange interaction [25]. Moreover, the Cr2-Te1-Cr3 bond angle within the layer, measuring approximately 91.213° , indicates super-exchange interactions that favor ferromagnetism [64, 65]. Further the strong hybridization between Cr $3d$ and Te $5p$ orbitals potentially establishes an indirect exchange between the Cr moments mediated by neighboring Te atoms [66].

Finally, before concluding this section, we would like to mention that during the course of our manuscript preparation a preprint discussing the magnetocrystalline anisotropy and

magnetic interactions of $\text{Cr}_{1.77}\text{Te}_3$ (claimed as Cr_2Te_3) single crystals has appeared [67]. Though, our results of out-of-plane magnetization matches well with the Ref. [67], the in-plane magnetization is slightly different. Moreover, based on the magnetocaloric effect (MCE) analysis, Ref. [67] suggests a 2D-Ising type magnetic interactions in their studied composition of $\text{Cr}_{1.77}\text{Te}_3$ despite the experimentally obtained $\beta = 0.2435$ and $\gamma = 1.6509$ are quite far from the theoretically predicted values ($\beta = 0.125$ and $\gamma = 1.75$) for a 2D-Ising type magnet. Whereas, our studies demonstrate a complex magnetic interactions falling in between the 3D-Ising and 3D-Heisenberg models. We suggest that the difference in the type of magnetic interactions between our study and Ref. [67] is possibly related to the differing Cr concentrations.

3.5. Magnetocaloric Effect

The magnetocaloric effect that is inherent to ferromagnetic system, induces heating or cooling when the system is adiabatically subjected to the external magnetic fields [68]. This phenomenon results in a magnetic entropy change $-\Delta S_m(T, H)$ in the presence of magnetic fields, expressed by the formula,

$$\Delta S_m(T, H) = \int_0^H \left(\frac{\partial S}{\partial H}\right)_T dH = \int_0^H \left(\frac{\partial M}{\partial T}\right)_H dH \quad (13)$$

According to the Maxwell's relation, $\left(\frac{\partial S}{\partial H}\right)_T = \left(\frac{\partial M}{\partial T}\right)_H$. For the magnetization measured within small discrete fields and temperature intervals, $\Delta S_m(T, H)$ can be expressed as

$$\Delta S_m(T, H) = \frac{\int_0^H M(T_{i+1}, H) dH - \int_0^H M(T_i, H) dH}{T_{i+1} - T_i} \quad (14)$$

Fig. 8 displays the temperature dependence of derived $-\Delta S_m(T, H)$ for $H \parallel c$ at different magnetic field strength. These curves showcase a peak change in entropy around T_C , presenting a broad peak pattern. At 6 T of applied field $-\Delta S_m(T, H)$ reaches maximum of approximately $2.08 \text{ J kg}^{-1} \text{ K}^{-1}$ for $H \parallel c$. The observed $-\Delta S_m(T, H)$ values at 6 T are comparable to those obtained from other 2D magnetic materials such as $\text{Cr}_2\text{Ge}_2\text{Te}_6$ ($2.64 \text{ J kg}^{-1} \text{ K}^{-1}$) [35] and Cr_5Te_8 ($2.38 \text{ J kg}^{-1} \text{ K}^{-1}$) [13], larger than $\text{Fe}_{3-x}\text{GeTe}_2$ ($1.14 \text{ J kg}^{-1} \text{ K}^{-1}$) [69] and CrI_3 ($1.56 \text{ J kg}^{-1} \text{ K}^{-1}$) [70], and smaller than CrB_3 ($7.2 \text{ J kg}^{-1} \text{ K}^{-1}$) [71] and $\text{Cr}_2\text{Si}_2\text{Te}_6$ ($5.05 \text{ J kg}^{-1} \text{ K}^{-1}$) [35].

4. Summary

We have successfully grown high-quality single crystals of Cr_2Te_3 using the chemical vapor transport method. Our investigation on the critical behavior of Cr_2Te_3 across the ferromagnetic to paramagnetic (FM-PM) transition temperature of 170 K, reveals crucial insights into the magnetic exchange interactions. Specifically, the Kouvel-Fisher (KF) method derives the critical exponents, $\beta = 0.353(4)$

and $\gamma=1.213(5)$, suggesting complex magnetic interactions falling in between the 3D-Ising and the 3D-Heisenberg models. Further, the renormalization group theory analysis indicates a 3D-Ising-type magnetic interactions decaying with the distance as $J(r) = r^{-4.89}$. Importantly, the uniaxial magnetocrystalline anisotropy (MAE) of $K_u = 2065 \text{ kJ/m}^3$ is the highest ever known experimental value in Cr_xTe_y type systems. We suggest that the 3D-Ising type magnetic interactions in Cr_2Te_3 are stabilized by the extremely large uniaxial MAE. Further, the DFT calculations predict large MAE of $K_u = 8230 \text{ kJ/m}^3$, leading to a ground state noncollinear ferromagnetic structure with dominant out-of-plane ferromagnetic and dominant in-plane antiferromagnetic Cr-spin arrangements. The self-consistent renormalization theory (SCR) suggests Cr_2Te_3 to be an out-of-plane itinerant ferromagnet. Investigating the magnetic entropy change, $-\Delta S_M^{\text{max}}$, as a function of temperature provided insights on the magnetocaloric effect in this system. These findings collectively lay a robust groundwork for advancing the magnetocaloric and spintronic technologies.

5. Acknowledgements

S.T. thank the Science and Engineering Research Board (SERB), Department of Science and Technology (DST), India for the financial support (Grant No. SRG/2020/000393). This research has made use of the Technical Research Centre (TRC) Instrument Facilities of S. N. Bose National Centre for Basic Sciences, established under the TRC project of the Department of Science and Technology, Govt. of India.

References

- [1] J. T. Heron, M. Trassin, K. Ashraf, M. Gajek, Q. He, S. Y. Yang, D. E. Nikonov, Y.-H. Chu, S. Salahuddin, R. Ramesh, Electric-Field-Induced Magnetization Reversal in a Ferromagnet-Multiferroic Heterostructure, *Phys. Rev. Lett.* 107 (2011) 217202.
- [2] A. K. Geim, I. V. Grigorieva, Van der Waals heterostructures, *Nature* 499 (2013) 419–425.
- [3] C. Gong, L. Li, Z. Li, H. Ji, A. Stern, Y. Xia, T. Cao, W. Bao, C. Wang, Y. Wang, et al., Discovery of intrinsic ferromagnetism in two-dimensional van der Waals crystals, *Nature* 546 (2017) 265–269.
- [4] Z. Fei, B. Huang, P. Malinowski, W. Wang, T. Song, J. Sanchez, W. Yao, D. Xiao, X. Zhu, A. F. May, et al., Two-dimensional itinerant ferromagnetism in atomically thin Fe_3GeTe_2 , *Nat. Mater.* 17 (2018) 778–782.
- [5] B. Wang, Y. Zhang, L. Ma, Q. Wu, Y. Guo, X. Zhang, J. Wang, MnX ($X = \text{P, As}$) monolayers: a new type of two-dimensional intrinsic room temperature ferromagnetic half-metallic material with large magnetic anisotropy, *Nanoscale* 11 (2019) 4204–4209.
- [6] M. Gibertini, M. Koperski, A. F. Morpurgo, K. S. Novoselov, Magnetic 2D materials and heterostructures, *Nat. Nanotechnol.* 14 (2019) 408–419.
- [7] N. D. Mermin, H. Wagner, Absence of Ferromagnetism or Antiferromagnetism in One- or Two-Dimensional Isotropic Heisenberg Models, *Phys. Rev. Lett.* 17 (1966) 1133–1136.
- [8] B. Huang, G. Clark, E. Navarro-Moratalla, D. R. Klein, R. Cheng, K. L. Seyler, D. Zhong, E. Schmidgall, M. A. McGuire, D. H. Cobden, W. Yao, D. Xiao, P. Jarillo-Herrero, X. Xu, Layer-dependent ferromagnetism in a van der Waals crystal down to the monolayer limit, *Nature* 546 (2017) 270–273.
- [9] Y. Liu, C. Petrovic, Critical behavior of quasi-two-dimensional semiconducting ferromagnet $\text{Cr}_2\text{Ge}_2\text{Te}_6$, *Phys. Rev. B* 96 (2017) 054406.
- [10] T. J. Williams, A. A. Aczel, M. D. Lumsden, S. E. Nagler, M. B. Stone, J.-Q. Yan, D. Mandrus, Magnetic correlations in the quasi-two-dimensional semiconducting ferromagnet CrSiTe_3 , *Phys. Rev. B* 92 (2015) 144404.
- [11] L.-Z. Zhang, A.-L. Zhang, X.-D. He, X.-W. Ben, Q.-L. Xiao, W.-L. Lu, F. Chen, Z. Feng, S. Cao, J. Zhang, J.-Y. Ge, Critical behavior and magnetocaloric effect of the quasi-two-dimensional room-temperature ferromagnet Cr_4Te_5 , *Phys. Rev. B* 101 (2020) 214413.
- [12] Y. Wang, S. Kajihara, H. Matsuoka, B. K. Saika, K. Yamagami, Y. Takeda, H. Wadati, K. Ishizaka, Y. Iwasa, M. Nakano, Layer-Number-Independent Two-Dimensional Ferromagnetism in Cr_3Te_4 , *Nano Lett.* 22 (2022) 9964.
- [13] Y. Liu, M. Abeykoon, E. Stavitski, K. Attenkofer, C. Petrovic, Magnetic anisotropy and entropy change in trigonal Cr_5Te_8 , *Phys. Rev. B* 100 (2019) 245114.
- [14] T. Hashimoto, M. Yamaguchi, Magnetic Properties of Cr_7Te_8 , *J. Phys. Soc. Jpn.* 27 (1969) 1121–1126.
- [15] L.-Z. Zhang, Q.-L. Xiao, F. Chen, Z. Feng, S. Cao, J. Zhang, J.-Y. Ge, Multiple magnetic phase transitions and critical behavior in single crystal Cr_5Te_6 , *J. Magn. Magn. Mater.* 546 (2022) 168770.
- [16] H. Liu, H. Zheng, Y. Wang, C. Huang, C. Ma, Y. Zhu, H. Yang, L. Ling, L. Zhang, J. Fan, Long-range magnetic exchange coupling in quasi-two-dimensional CrTe ferromagnetic thin films, *Physica Status Solidi (RRL)–Rapid Research Letters* 17 (2023) 202300209.
- [17] M. Yamaguchi, T. Hashimoto, Magnetic properties of Cr_3Te_4 in ferromagnetic region, *J. Phys. Soc. Jpn.* 32 (1972) 635–638.
- [18] G. Chattopadhyay, The Cr-Te (chromium-tellurium) system, *J. Phase Equilib.* 15 (1994) 431–440.
- [19] S. Purwar, A. Low, A. Bose, A. Narayan, S. Thirupathiah, Investigation of the anomalous and topological Hall effects in layered monoclinic ferromagnet $\text{Cr}_{2.76}\text{Te}_4$, *Phys. Rev. Materials* 7 (2023) 094204.
- [20] D. C. Freitas, R. Weht, A. Sulpice, G. Remenyi, P. Strobel, F. Gay, J. Marcus, M. Núñez-Regueiro, Ferromagnetism in layered metastable 1T-CrTe₂, *J. Phys.: Condens. Matter* 27 (2015) 176002.
- [21] M. Bian, A. N. Kamenskii, M. Han, W. Li, S. Wei, X. Tian, D. B. Eason, F. Sun, K. He, H. Hui, et al., Covalent 2D Cr_2Te_3 ferromagnet, *Mater. Res. Lett.* 9 (2021) 205–212.
- [22] H. Ipsier, K. L. Komarek, K. O. Klepp, Transition metal-chalcogen systems viii: The CrTe phase diagram, *Journal of the Less Common Metals* 92 (1983) 265–282.
- [23] M. A. McGuire, V. O. Garlea, S. KC, V. R. Cooper, J. Yan, H. Cao, B. C. Sales, Antiferromagnetism in the van der Waals layered spinlozenge semiconductor CrTe_3 , *Phys. Rev. B* 95 (2017) 144421.
- [24] R. Mondal, R. Kulkarni, A. Thamizhavel, Anisotropic magnetic properties and critical behaviour studies of trigonal Cr_5Te_8 single crystal, *J. Magn. Magn. Mater.* 483 (2019) 27–33.
- [25] Z. Jiang, X. Liang, X. Luo, J. Gao, W. Wang, T. Wang, X. Yang, X. Wang, L. Zhang, Y. Sun, et al., Evolution of ground state in Cr_2Te_3 single crystal under applied magnetic field, *Phys. Rev. B* 106 (2022) 094407.
- [26] Y. Wen, Z. Liu, Y. Zhang, C. Xia, B. Zhai, X. Zhang, G. Zhai, C. Shen, P. He, R. Cheng, et al., Tunable room-temperature ferromagnetism in two-dimensional Cr_2Te_3 , *Nano Lett.* 20 (2020) 3130–3139.
- [27] F.-S. Luo, J.-S. Ying, T.-W. Chen, F. Tang, D.-W. Zhang, W.-Q. Dong, Y. Zhang, S.-S. Li, Y. Fang, R.-K. Zheng, Anomalous Hall effect and anisotropic magnetoresistance of molecular beam epitaxy grown Cr_2Te_3 thin films, *J. Cryst. Growth* 582 (2022) 126541.
- [28] J. H. Jeon, H. R. Na, H. Kim, S. Lee, S. Song, J. Kim, S. Park, J. Kim, H. Noh, G. Kim, et al., Emergent topological Hall effect from exchange coupling in ferromagnetic Cr_2Te_3 /Noncoplanar antiferromagnetic Cr_2Te_3 bilayers, *ACS nano* 16 (2022) 8974–8982.
- [29] N. Abuawwad, M. dos Santos Dias, H. Abusara, S. Lounis, Noncollinear magnetism in two-dimensional CrTe_2 , *Journal of Physics: Condensed Matter* 34 (2022) 454001.

- [30] T. Hashimoto, K. Hoya, M. Yamaguchi, I. Ichitsubo, Magnetic properties of single crystals $\text{Cr}_{2-6}\text{Te}_3$, *J. Phys. Soc. Jpn.* 31 (1971) 679–682.
- [31] J. P. Perdew, K. Burke, M. Ernzerhof, Generalized Gradient Approximation Made Simple, *Phys. Rev. Lett.* 77 (1996) 3865–3868.
- [32] P. Giannozzi, S. Baroni, N. Bonini, M. Calandra, R. Car, C. Cavazzoni, D. Ceresoli, G. L. Chiarotti, M. Cococcioni, I. Dabo, et al., QUANTUM ESPRESSO: a modular and open-source software project for quantum simulations of materials, *J. Phys.: Condens. Matter* 21 (2009) 395502.
- [33] T. Hamasaki, T. Hashimoto, Y. Yamaguchi, H. Watanabe, Neutron diffraction study of Cr_2Te_3 single crystal, *Solid State Commun.* 16 (1975) 895–897.
- [34] A. F. ANDRESEN, E. Zeppezauer, T. Boive, B. Nordström, C. Brändén, Magnetic structure of Cr_2Te_3 , Cr_3Te_4 , and Cr_5Te_6 , *Acta Chem. Scand.* 24 (1970) 3495–3509.
- [35] Y. Liu, C. Petrovic, Anisotropic magnetic entropy change in $\text{Cr}_2\text{X}_2\text{Te}_6$ ($X = \text{Si}$ and Ge), *Phys. Rev. Materials* 3 (2019) 014001.
- [36] S. Mondal, N. Khan, S. M. Mishra, B. Satpati, P. Mandal, Critical behavior in the van der Waals itinerant ferromagnet Fe_4GeTe_2 , *Phys. Rev. B* 104 (2021) 094405.
- [37] N. Richter, D. Weber, F. Martin, N. Singh, U. Schwingenschlögl, B. V. Lotsch, M. Kläui, Temperature-dependent magnetic anisotropy in the layered magnetic semiconductors CrI_3 and CrBr_3 , *Phys. Rev. Materials* 2 (2018) 024004.
- [38] N. León-Brito, E. D. Bauer, F. Ronning, J. D. Thompson, R. Movshovich, Magnetic microstructure and magnetic properties of uniaxial itinerant ferromagnet Fe_3GeTe_2 , *J. Appl. Phys.* 120 (2016) 083903.
- [39] Y. Takahashi, Spin fluctuation theory of itinerant electron magnetism, volume 9, Springer, 2013. URL: <https://doi.org/10.1007/978-3-642-36666-6>, doi:10.1007/978-3-642-36666-6.
- [40] M. Chattopadhyay, P. Arora, S. Roy, Magnetic properties of the field-induced ferromagnetic state in MnSi , *J. Phys.: Condens. Matter* 21 (2009) 296003.
- [41] M. Imai, C. Michioka, H. Ueda, K. Yoshimura, Static and dynamical magnetic properties of the itinerant ferromagnet LaCo_2P_2 , *Phys. Rev. B* 91 (2015) 184414.
- [42] H. Ohta, C. Michioka, A. Matsuo, K. Kindo, K. Yoshimura, Magnetic study of SmCoAsO showing a ferromagnetic-antiferromagnetic transition, *Phys. Rev. B* 82 (2010) 054421.
- [43] A. Arrott, Criterion for Ferromagnetism from Observations of Magnetic Isotherms, *Phys. Rev.* 108 (1957) 1394–1396.
- [44] H. E. Stanley, Phase transitions and critical phenomena, volume 7, Clarendon Press, Oxford, 1971.
- [45] S. Kaul, Static critical phenomena in ferromagnets with quenched disorder, *J. Magn. Magn. Mater.* 53 (1985) 5–53.
- [46] D. Kim, B. Revaz, B. L. Zink, F. Hellman, J. J. Rhyne, J. F. Mitchell, Tricritical Point and the Doping Dependence of the Order of the Ferromagnetic Phase Transition of $\text{La}_{1-x}\text{Ca}_x\text{MnO}_3$, *Phys. Rev. Lett.* 89 (2002) 227202.
- [47] Y. Liu, C. Petrovic, Critical behavior of the quasi-two-dimensional weak itinerant ferromagnet trigonal chromium telluride $\text{Cr}_{0.62}\text{Te}$, *Phys. Rev. B* 96 (2017) 134410.
- [48] A. Wang, A. Rahman, Z. Du, J. Zhao, F. Meng, W. Liu, J. Fan, C. Ma, M. Ge, L. Pi, et al., Field-dependent anisotropic room-temperature ferromagnetism in Cr_3Te_4 , *Phys. Rev. B* 108 (2023) 094429.
- [49] M. E. Fisher, The theory of equilibrium critical phenomena, *Reports on progress in physics* 30 (1967) 615.
- [50] J. C. Le Guillou, J. Zinn-Justin, Critical exponents from field theory, *Phys. Rev. B* 21 (1980) 3976–3998.
- [51] A. Arrott, J. E. Noakes, Approximate equation of state for nickel near its critical temperature, *Phys. Rev. Lett.* 19 (1967) 786–789.
- [52] A. K. Pramanik, A. Banerjee, Critical behavior at paramagnetic to ferromagnetic phase transition in $\text{Pr}_{0.5}\text{Sr}_{0.5}\text{MnO}_3$: A bulk magnetization study, *Phys. Rev. B* 79 (2009) 214426.
- [53] J. S. Kouvel, M. E. Fisher, Detailed Magnetic Behavior of Nickel Near its Curie Point, *Phys. Rev.* 136 (1964) A1626–A1632.
- [54] B. Widom, Degree of the critical isotherm, *J. Chem. Phys.* 41 (1964) 1633–1634.
- [55] S. N. Kaul, Detailed magnetization study of an amorphous ferromagnet, *Phys. Rev. B* 24 (1981) 6550–6565.
- [56] N. Tateiwa, Y. Haga, T. D. Matsuda, E. Yamamoto, Z. Fisk, Unconventional critical scaling of magnetization in ferromagnetic uranium superconductors UGe_2 and URhGe , *Phys. Rev. B* 89 (2014) 064420.
- [57] X. Yang, J. Pan, S. Liu, M. Yang, L. Cao, D. Chu, K. Sun, Critical behavior and anisotropic magnetocaloric effect of the quasi-one-dimensional hexagonal ferromagnet PrCrGe_3 , *Phys. Rev. B* 103 (2021) 104405.
- [58] Y. Liu, Z. Hu, E. Stavitski, K. Attenkofer, C. Petrovic, Magnetic critical behavior and anomalous Hall effect in $2\text{H}-\text{Co}_{0.22}\text{TaS}_2$ single crystals, *Phys. Rev. Res.* 3 (2021) 023181.
- [59] X. Yang, J. Pan, W. Gai, Y. Tao, H. Jia, L. Cao, Y. Cao, Three-dimensional critical behavior and anisotropic magnetic entropy change in quasi-two-dimensional LaCrSb_3 , *Phys. Rev. B* 105 (2022) 024419.
- [60] S. F. Fischer, S. N. Kaul, H. Kronmüller, Critical magnetic properties of disordered polycrystalline $\text{Cr}_{75}\text{Fe}_{25}$ and $\text{Cr}_{70}\text{Fe}_{30}$ alloys, *Phys. Rev. B* 65 (2002) 064443.
- [61] M. E. Fisher, S.-k. Ma, B. G. Nickel, Critical Exponents for Long-Range Interactions, *Phys. Rev. Lett.* 29 (1972) 917–920.
- [62] X. Zhang, T. Yu, Q. Xue, M. Lei, R. Jiao, Critical behavior and magnetocaloric effect in monoclinic Cr_5Te_8 , *J. Alloys Compd.* 750 (2018) 798–803.
- [63] S. Youn, S. Kwon, B. Min, Correlation effect and magnetic moments in Cr_2Te_3 , *J. Appl. Phys.* 101 (2007) 09G522.
- [64] J. B. Goodenough, Theory of the role of covalence in the perovskite-type manganites [$\text{La}, \text{M}(\text{II})$] $\text{MnO}-3$, *Phys. Rev.* 100 (1955) 564.
- [65] J. Kanamori, Superexchange interaction and symmetry properties of electron orbitals, *J. Phys. Chem. Solids* 10 (1959) 87–98.
- [66] J. Dijkstra, H. H. Weitering, C. F. van Bruggen, C. Haas, R. A. de Groot, Band-structure calculations, and magnetic and transport properties of ferromagnetic chromium tellurides ($\text{CrTe}, \text{Cr}_3\text{Te}_4, \text{Cr}_2\text{Te}_3$), *J. Phys.: Condens. Matter* 1 (1989) 9141–9161.
- [67] A. Goswami, N. Ng, A. M. Abeykoon, E. Yakubu, S. Guchhait, High magnetic anisotropy and magnetocaloric effects in single crystal Cr_2Te_3 , 2023. [arXiv:2312.01000](https://arxiv.org/abs/2312.01000).
- [68] V. K. Pecharsky, K. A. Gschneidner Jr, Magnetocaloric effect and magnetic refrigeration, *J. Magn. Magn. Mater.* 200 (1999) 44–56.
- [69] Y. Liu, J. Li, J. Tao, Y. Zhu, C. Petrovic, Anisotropic magnetocaloric effect in $\text{Fe}_{3-x}\text{GeTe}_3$, *Sci. Rep.* 9 (2019) 13233.
- [70] Y. Liu, C. Petrovic, Anisotropic magnetocaloric effect in single crystals of CrI_3 , *Phys. Rev. B* 97 (2018) 174418.
- [71] X. Yu, X. Zhang, Q. Shi, S. Tian, H. Lei, K. Xu, H. Hosono, Large magnetocaloric effect in van der Waals crystal CrBr_3 , *Front. Phys.-Beijing.* 14 (2019) 43501.